Supplementary Material

Multifunctional approach to improve water oxidation performance with MOF-based photoelectrodes

Niloufar Afzali[1], Reza Keshavarzi[1]*, Shahram Tangestaninejad[1]*, *Sixto Gimenez*[2]*, Valiollah Mirkhani[1], Majid Moghadam[1], Iraj Mohammadpoor-Baltork[1]

[1]*Department of Chemistry, Catalysis Division, University of Isfahan, Isfahan 81746-73441, Iran*

[2]*Photovoltaics and Optoelectronic Devices Group, Departament de Física, Universitat Jaume I, 12071 Castelló, Spain*

Reza Keshavarzi; Email: R.keshavarzi@Chem.ui.ac.ir

Shahram Tangestaninejad; Email: Stanges@sci.ui.ac.ir

Sixto Giménez: Email: sjulia@uji.es

Number of pages: 9

Number of tables: 2

Number of figures: 15

Contents:

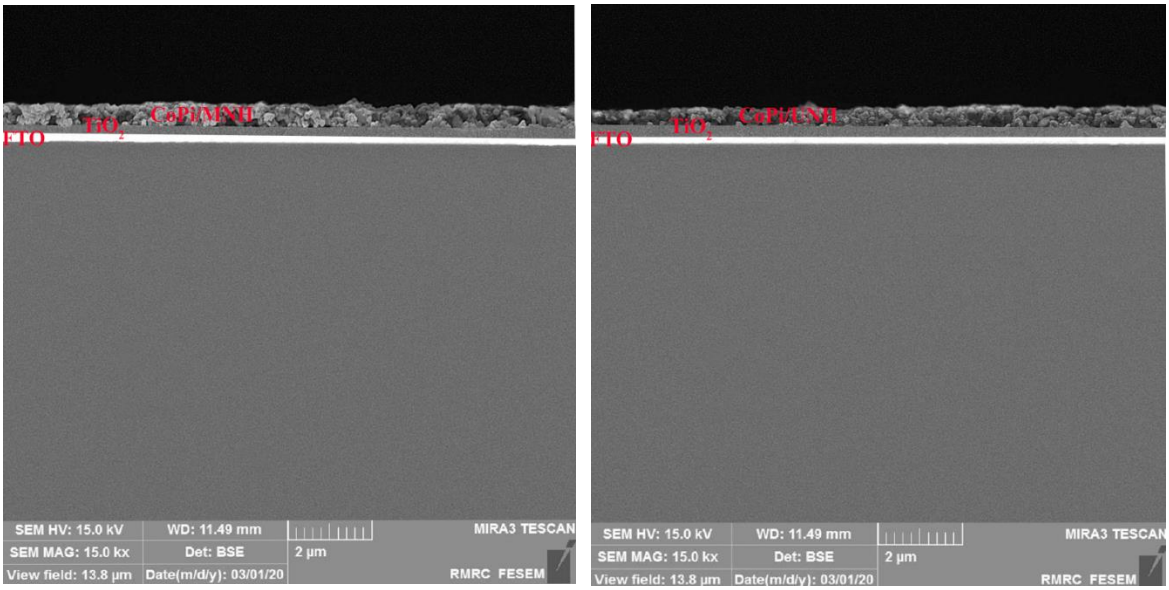

Figure S1. Cross-section view of CoPi/MNH/TiO_2 and CoPi/UNH/TiO_2.

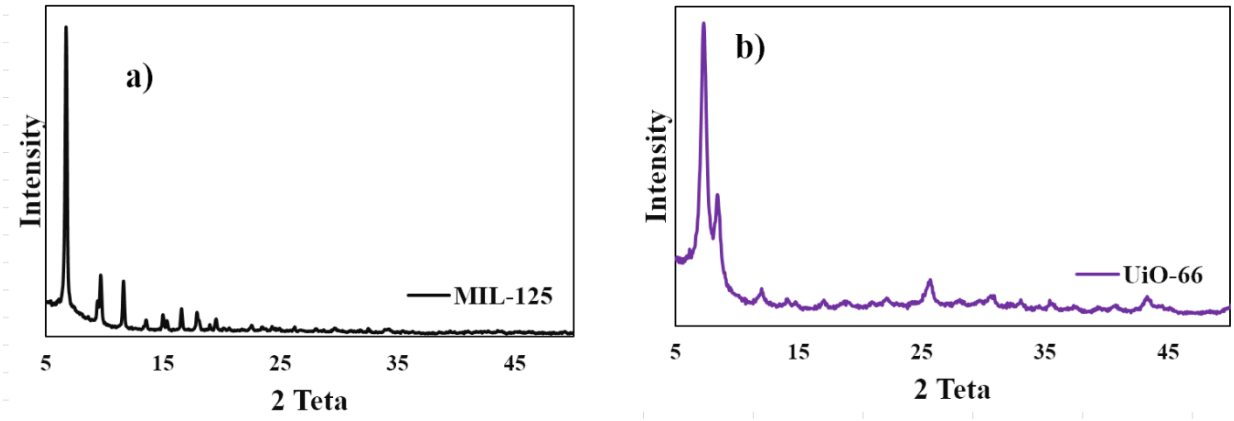

Figure S2. Powder XRD patterns of a) UIO-66 and b) MIL-125.

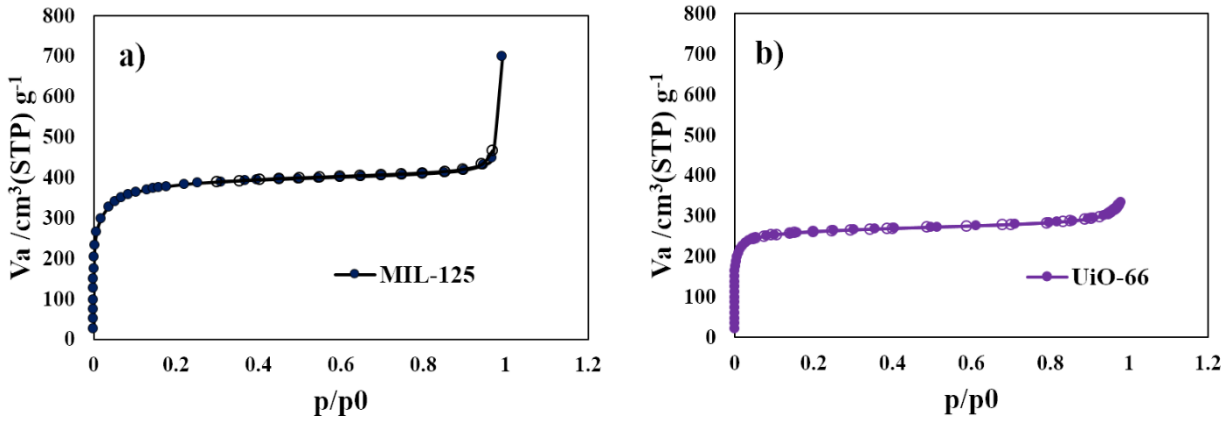

Figure S3. BET surface area analysis: Adsorption-desorption isotherms of the UiO-66 and MIL-125 (a and b).

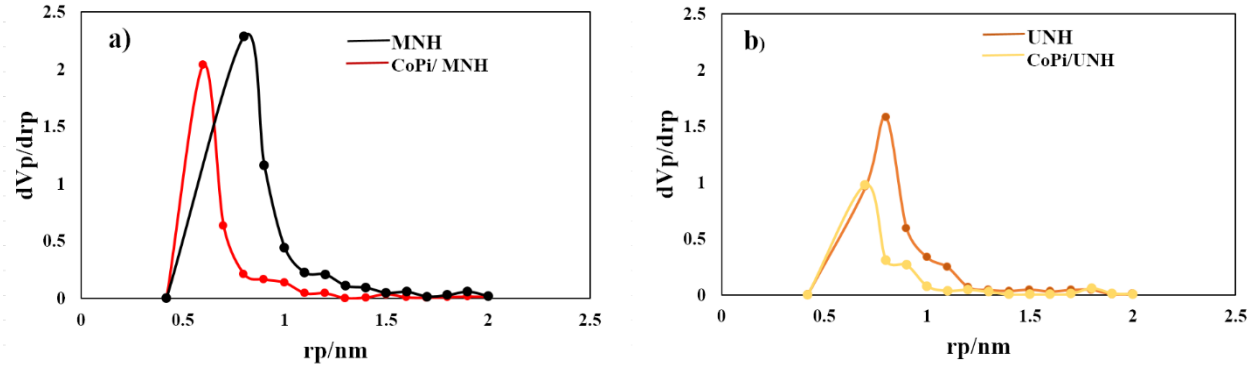

Figure S4. Related pore size distributions for MOF photo catalyst, calculated from MP plots (micropores range).

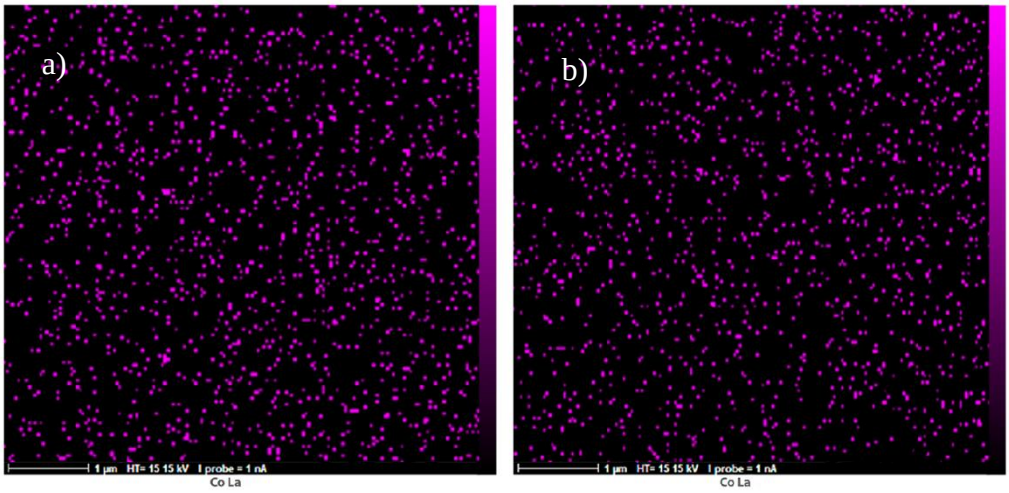

Figure S5. Elemental mapping for CoPi/ MNH (a) and CoPi/ UNH (b).

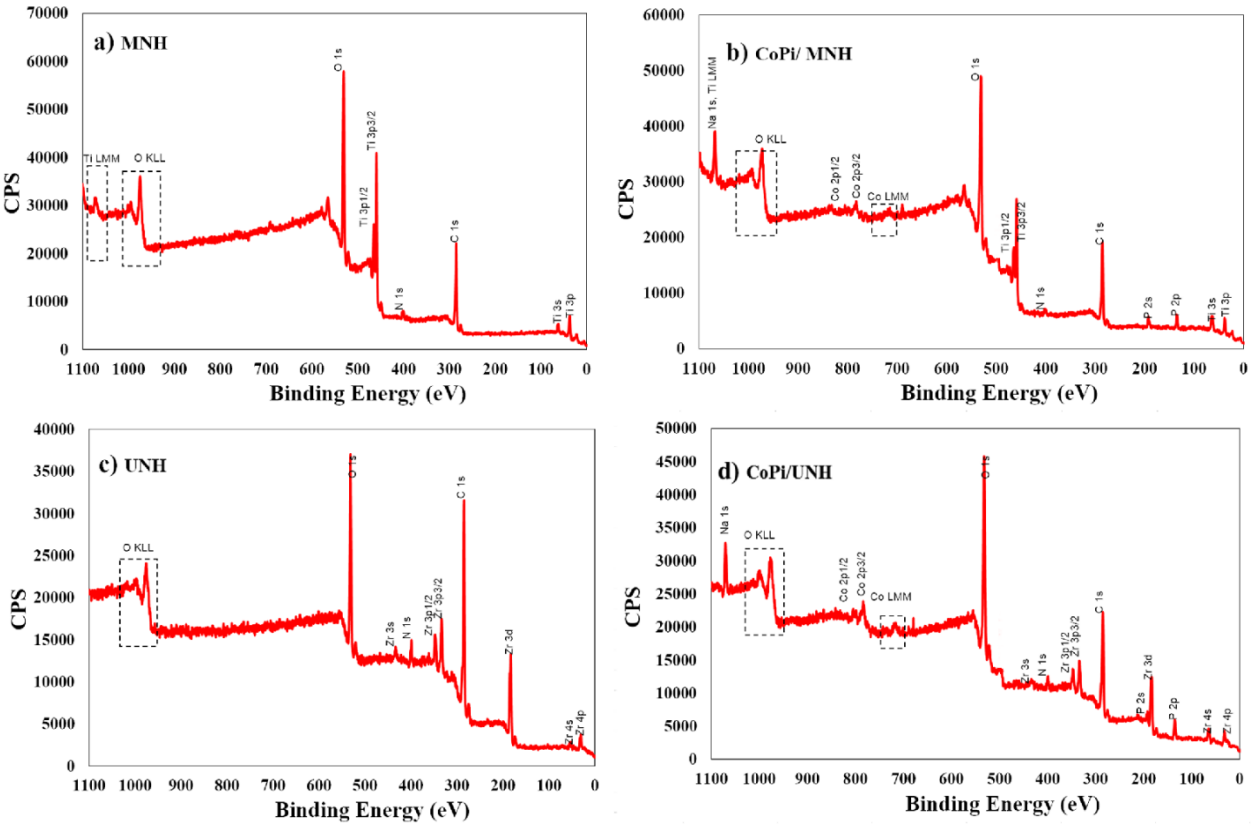

Figure S6. X-ray photoelectron spectroscopy (XPS) analysis, full scan spectrum of (a) CoPi/ MNH (right), and MNH (left), and (b) CoPi/ UNH (right) and UNH(left).

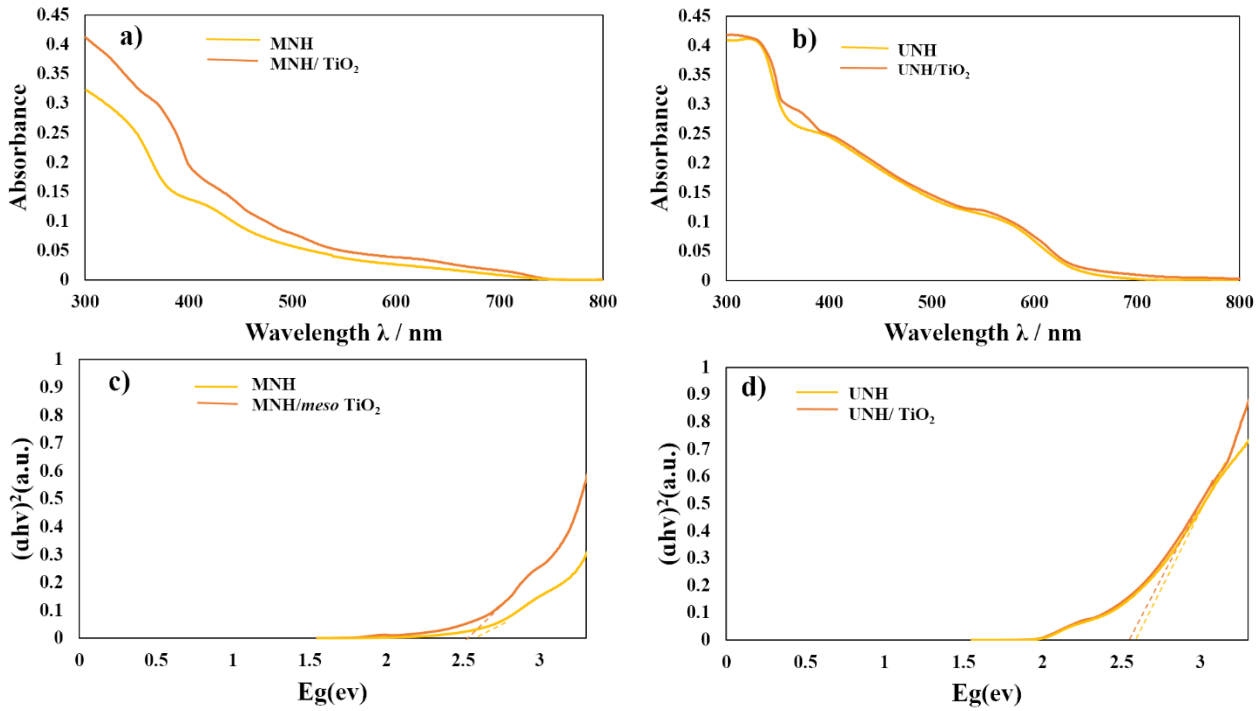

Figure S7. UV-Vis absorption spectra (a and b), and Tauc plots for indirect band gap determination of MOF composites (c and d).

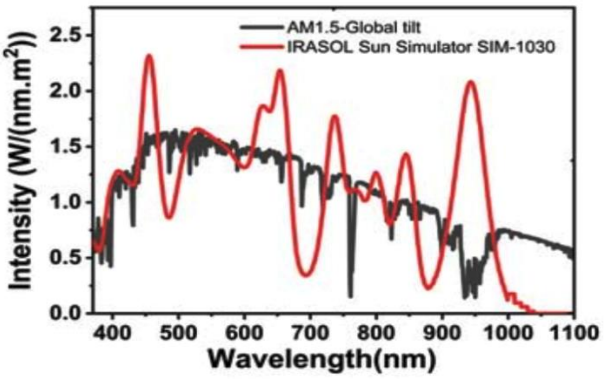

Figure S8. The wavelength spectrum of solar simulator (380-1100nm).

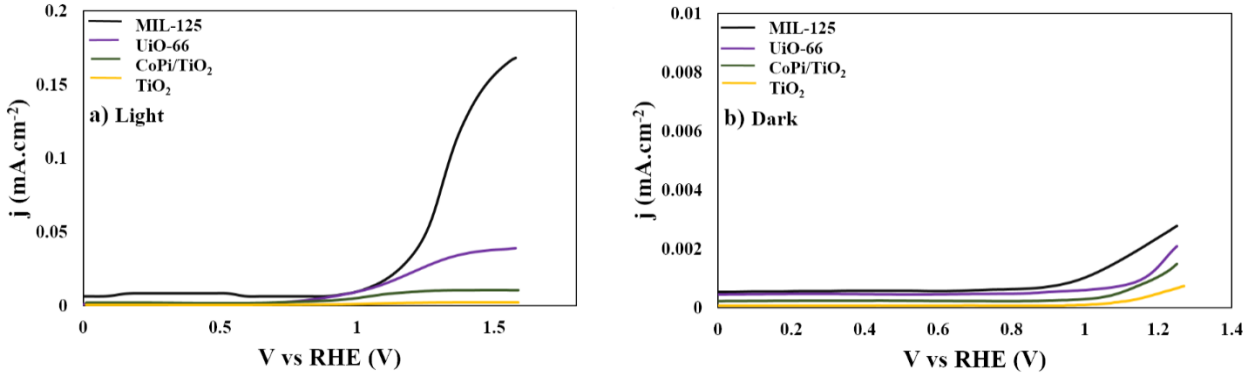

Figure S9. Linear sweep photovoltammograms of MIL-125, UiO-66, $CoPi/TiO_2$ and TiO_2 in artificial seawater electrolyte a) under illumination at 100 $mW \cdot cm^{-2}$ and b) in dark.

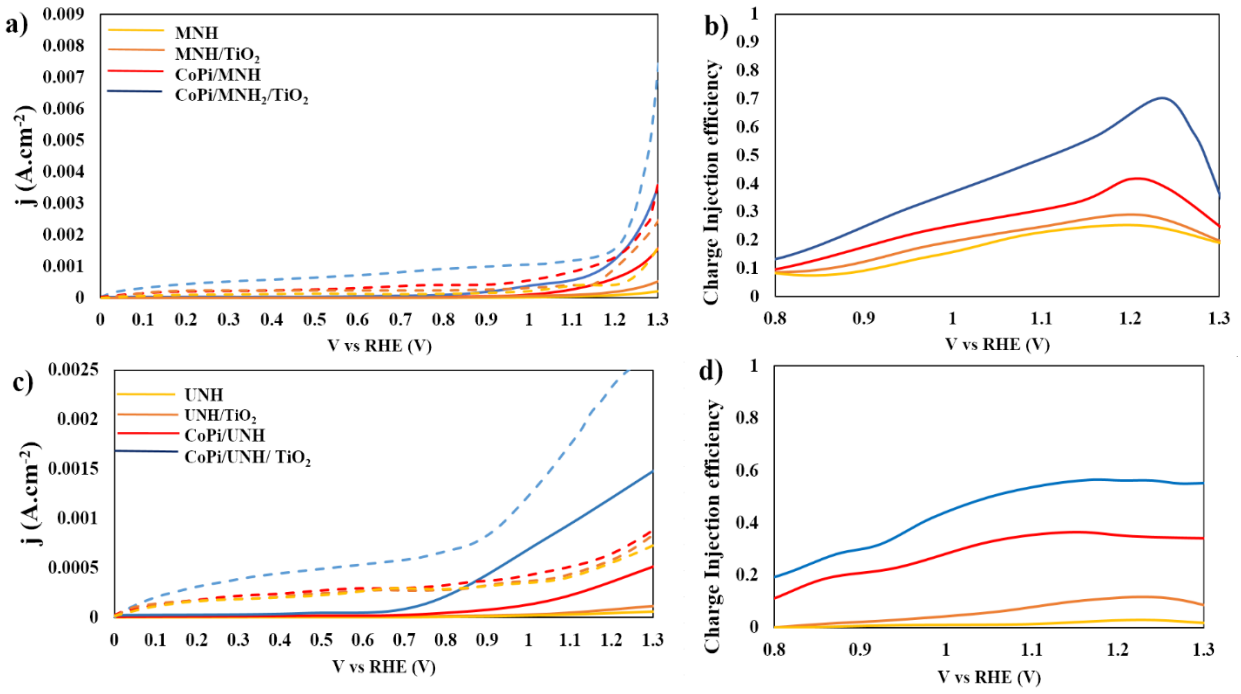

Figure S10: Calculated charge-injection efficiencies of photoelectrodes (j-V curves of the samples in the presence of a hole scavenger (0.5M Na_2SO_3)) without (line) and with (dash line) illumination.

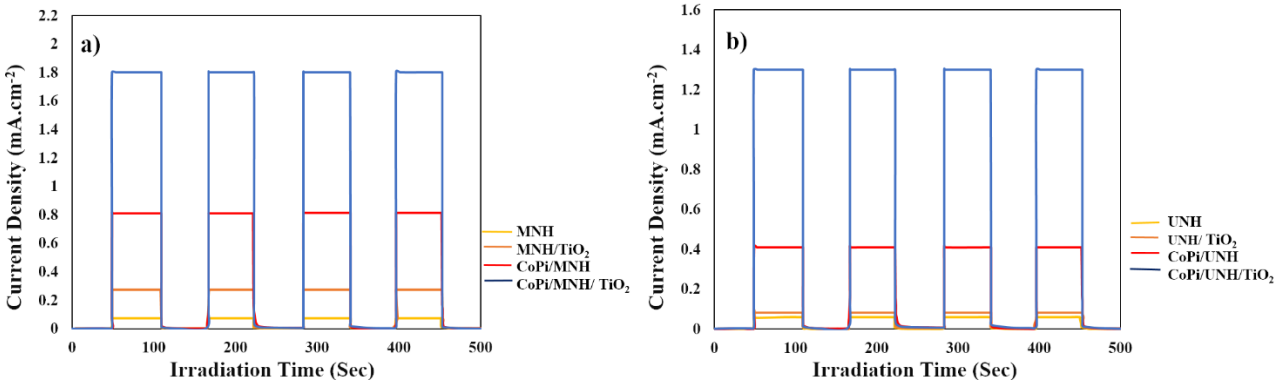

Figure. S11. Transient photoelectrochemical measurements of MOFs composite at 1.23V vs RHE.

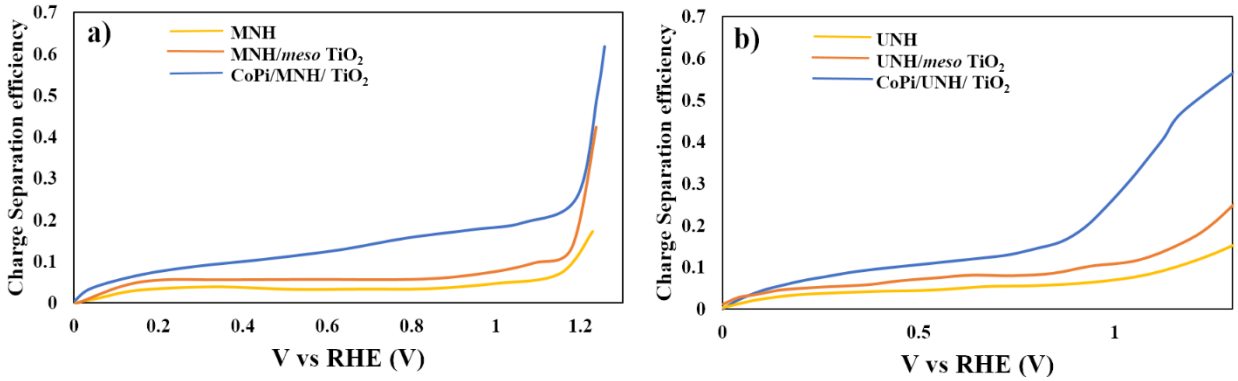

Figure S12. Calculated charge-separation efficiencies of photoelectrodes.

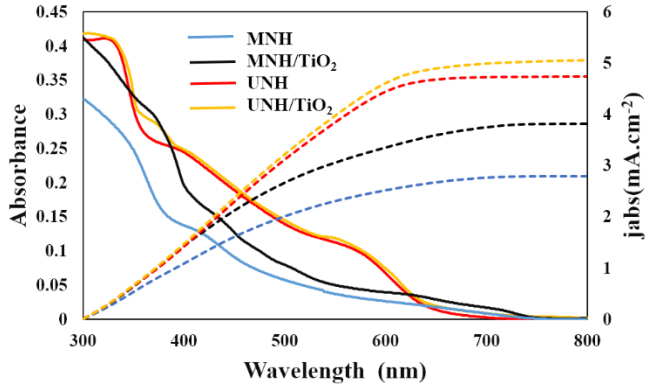

Figure S13. The maximum theoretical photocurrent extracted after integration of the calculated absoroptance ($a = 1 - 10^{-A}$).

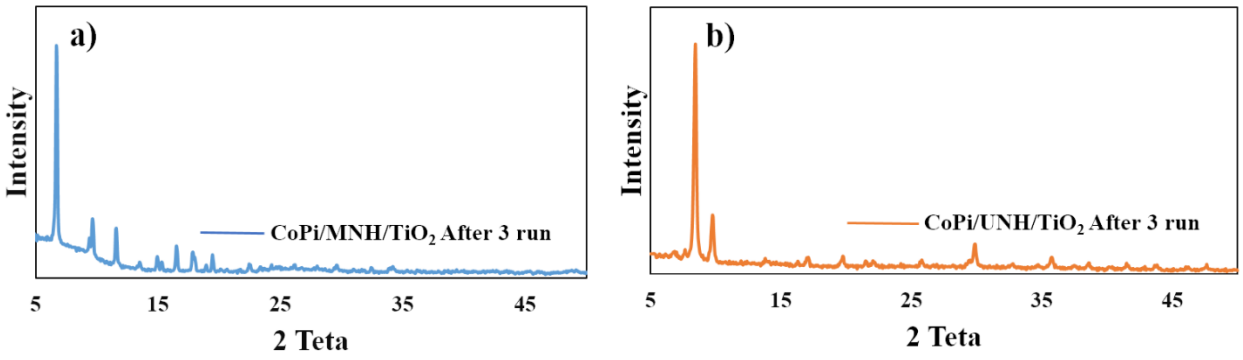

Figure S14. Powder XRD patterns of photoelectrodes after photoelectrochemical testing (3 runs).

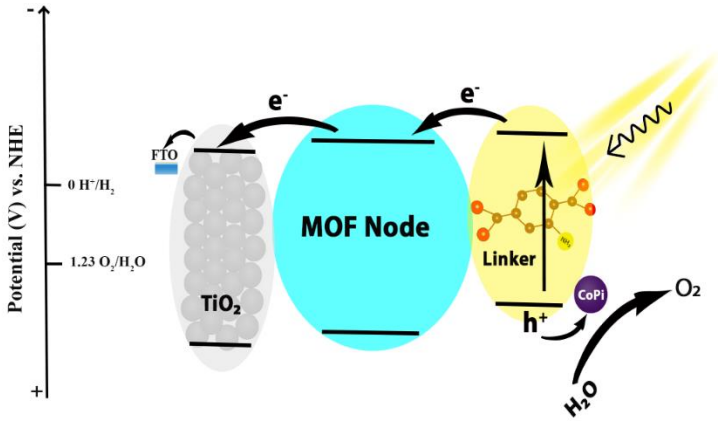

Figure S15. A schematic illustration of photocatalytic water oxidation mechanism over CoPi/MOF/TiO_2 samples.

Table S1. Results of energy-dispersive X-ray spectroscopy of CoPi/ MNH and CoPi/ UNH.

element	C(wt%)	Ti(wt%)	Zr(wt%)	O(wt%)	N(wt%)	Co(wt%)	P(wt%)
CoPi/ MNH	45.5	9.4	-	31.1	2.8	6.1	5.1
CoPi/ UNH	44.8	-	9.1	30.5	2.5	7.1	6

Table S2. Elemental ratios from XPS analysis.

Sample	C	N	O	Zr	Ti	Co	P
MNH	44.428	4.185	38.191	-	13.196	-	-
CoPi/ MNH	34.689	2.059	41.682	-	8.668	1.505	5.126
UNH	64.617	4.56	25.862	4.961	-	-	-
CoPi/ UNH	45.463	2.975	34.846	3.89	-	2.357	5.69